Available online at www.sciencedirect.com
SCIENCE DIRECT®
Journal of Computational Physics 217 (2006) 82–99
JOURNAL OF COMPUTATIONAL PHYSICS
www.elsevier.com/locate/jcp

Covariance kernel representations of multidimensional second-order stochastic processes

C.H. Su [a], Didier Lucor [b,*]

[a] Center for Fluid Mechanics, Turbulence and Computation, Division of Applied Mathematics, Brown University, Providence, RI 02912, United States
[b] Laboratoire de Modélisation en Mécanique, Université Pierre et Marie Curie, 4 Place Jussieu, Case 162, 75252 Paris, France

Received 3 August 2005; received in revised form 2 February 2006; accepted 9 February 2006
Available online 31 March 2006

Abstract

The dynamics of stationary stochastic processes in space is not exactly analogous to that of stationary stochastic processes in the time domain. This is due to the unilateral nature of the time series that is only influenced by past values as opposed to the dependence in all directions of the spatial process. In this work, we unfold the connection that exits between the covariance kernel of a multi-dimensional second-order autoregressive random process and its underlying discrete random dynamical system. Starting from a discrete random dynamical system, we show that the random process satisfying that system is governed by the modified Helmholtz equation in the continuous limit. We establish the dependence of the correlation constant on the grid size of the discretization. We also show that the random forcing term in the continuous case turns out to be a *white noise* process. A number of covariance functions are worked out for simple and more complex geometrical domains with various boundary conditions in multi-dimensions. We use both the discrete and the continuous systems in our computations.

Keywords: Uncertainty; Random inputs; Stochastic processes; Covariance kernel

1. Introduction

The need for a deep understanding and accurate representation of random inputs in computational stochastic modeling arose from a recent interest of the scientific community in studying *uncertainty quantification* (UQ) [1–3]. Random inputs are ubiquitous in engineering applications and include uncertainty in system parameters, boundary and initial conditions, material properties, source and interaction terms, geometry, etc. Random fields are used to model spatial data as observed for instance in environmental, ecological, meteorological, geological and hydro-geological sciences. Real life one-, two- or three-dimensional spatial random fields can be modeled by multi-dimensional stochastic processes (see for instance [4] for two-dimensional processes). In practice, it will often be the case that a few, if not just single, real realizations of a stochastic process

* Corresponding author. Tel.: +33 1 44 27 87 12.
E-mail address: lucor@lmm.jussieu.fr (D. Lucor).

0021-9991/$ - see front matter
doi:10.1016/j.jcp.2006.02.006

are given. Some particular assumptions must be made for the process to empower its numerical simulation with any practical use. The approximation of stationarity of the process is often regarded as a satisfactory approximation and make the study of the stationary type of stochastic process worth while. Another (stronger) assumption relates to the knowledge of its covariance matrix.

One approach is to model the random inputs as stochastic processes represented by functionals of idealized processes which typically correspond to *white noise* [5–7]. Another approach considers more realistic random inputs that are correlated random processes ("colored noise"). The particular case of random parameters, or fully correlated random processes, is referred as *random variables*.

One of the simplest and most used random processes is the first-order Markov process [8], which relates to the Brownian motion of small particles and the diffusion phenomenon. It is a unilateral type of scheme extended only in one direction and therefore very convenient for time-dependent random inputs and stochastic initial-valued problems [9]. The covariance kernel associated with that one-dimensional first-order autoregressive process takes an exponential form $a\exp(-|t_1 - t_2|/A)$ where A is the correlation time and a specifies the strength of the correlation [10]. In the limit of $\Delta t \to 0$, one obtains the Langevin equation for the Brownian motion and the covariance function given above. However, realistic models of random series *in space* require autoregressive schemes with dependence in *all* directions [11]. We refer to them as *multi-dimensional second-order stochastic processes*. In some cases, it has been shown that schemes of bilateral type in one dimension can be effectively reduced to a unilateral one [11]. In previous works [12,13], explicit expressions of one-dimensional covariance kernels associated with periodic second-order autoregressive processes were derived and represented with a *Karhunen–Loeve* (KL) decomposition. The KL expansion is a very powerful tool for representing stationary and non-stationary random processes with explicitly known covariance functions [14]. In [15], a bilateral stochastic process was numerically represented by a KL expansion in a two dimensional bounded domain.

In this article, we wish to make explicit the connection that exits between the covariance kernel of a multi-dimensional second-order random process and its underlying discrete random dynamical system. We show that the random process satisfying the dynamical system is governed by the *modified* Helmholtz equation in the continuous limit. This also establishes the dependence of the correlation constant on the grid size of the discretization. It provides the nature of the random forcing for the discrete and the continuous system. We first review the one dimensional case and derive the analytic covariance functions of the random processes for different types of boundary conditions. We then derive the modified Helmholtz equation and solve it to compute the covariance functions again. We compare analytical and numerical solutions. The procedure is generalized to higher dimensions in the following section. A number of covariance functions are worked out for some simple and more complex geometrical domains. Both the discrete and the continuous systems are used. Finally, we conclude by pointing out the analogy that exist between the eigenfunctions expansion and the KL representation.

2. Derivation of the covariance kernel and corresponding modified Helmholtz equation in 1D

Let us consider the following discrete set of random variables $v_1, v_2, \ldots, v_q$ each associated with one of the q evenly distributed points $x_1, x_2, \ldots, x_q$ on a line. The set of variables ξ_i's are supposed to be finite independent identically-distributed (iid) random variables with zero mean and unit variance. The system is assumed to be *periodic*. The random variables v_i's are defined by the following (dynamical) system:

$$v_i = \frac{c}{2}(v_{i+1} + v_{i-1}) + a\xi_i \quad \text{with } i = 1, 2, \ldots, q, \tag{1}$$

where we take $v_{q+1} = v_1$ and $v_0 = v_q$ because of the periodicity. The parameter c is a constant correlation coefficient and a is a measure of the strength of the stochastic forcing. This system is called a (bilateral) second-order autoregressive process. Our goal is to compute the covariance kernel $C = \langle v_i v_j \rangle$ of the random process. This is done in the limit where $\Delta x \to 0$ or $q \to \infty$ for a fixed periodic length of L. First we relate this random process to the solution of a partial differential equation (the modified Helmholtz equation). Then, we construct the covariance function C of the process for one spatial dimension and for two and three spatial dimensions (next section).

Formally, we can write the solution of Eq. (1) as:

$$v_i = \sum_{j=1}^{q} \alpha_{ij} \xi_j. \tag{2}$$

With the periodic assumption, the coefficient matrix of v_i is translational invariant. The solution matrix α, in Eq. (2) will also be translational invariant. It will be defined by q instead of $q \times q$ elements. Let us define:

$$v_1 = \sum_{j=1}^{q} s_j \xi_j, \tag{3}$$

then

$$v_i = \sum_{j=1}^{q} s_j \xi_{j+i-1} = \sum_{k=i}^{k=q+i-1} s_{k-i+1} \xi_k. \tag{4}$$

Substituting Eq. (4) into Eq. (1) and making use of the orthonormal properties of the ξ_i, i.e. $\langle \xi_i \xi_j \rangle = \delta_{ij}$, we have:

$$\begin{aligned} s_1 &= \frac{c}{2}(s_2 + s_q) + a, \\ s_i &= \frac{c}{2}(s_{i+1} + s_{i-1}) \quad \text{for } i = 2, 3, \ldots, q \end{aligned} \tag{5}$$

with $s_{q+1} = s_1$ and $s_0 = s_q$ because of periodicity.

If q is an even integer (the derivation applies equally well to odd q without lack of generality), i.e., $q = 2p$, it is easy to show that:

$$s_{2p-k} = s_{k+2} \quad \text{for } k = 0, 1, 2 \ldots, p-2. \tag{6}$$

The system is then reduced to:

$$\begin{aligned} s_1 &= c s_2 + a, \\ s_2 &= \frac{c}{2}(s_3 + s_1), \\ &\vdots \\ s_p &= \frac{c}{2}(s_{p+1} + s_{p-1}), \\ s_{p+1} &= c s_p. \end{aligned} \tag{7}$$

This last set of equations is computed readily, by first calculating:

$$D_1 = 1 \text{ and } D_k = 2 - \frac{c^2}{D_{k-1}} \quad \text{for } k = 2, 3, \ldots, p, \tag{8}$$

and then:

$$s_1 = a \Big/ \left(1 - \frac{c^2}{D_p}\right) \quad \text{and} \quad s_k = \frac{c}{D_{p-k+2}} s_{k-1} \quad \text{for } k = 2, 3, \ldots, p+1. \tag{9}$$

Knowing s_i for $i = 1, 2, \ldots, q$, one can then reconstruct the α matrix in Eq. (2) and compute the covariance matrix:

$$C_{ij} = \langle v_i v_j \rangle = \sum_{k=1}^{q} \alpha_{ik} \alpha_{jk} = \sum_{k=1}^{q} s_k s_{k+|i-j|}. \tag{10}$$

Since the system is translational invariant, i.e., the process is *stationary*, C_{ii} is a constant. Let us consider the normalized covariance matrix C_{ij}/C_{ii} (we set $s_1 = 1$). Now c is the only free parameter. We need to

find a functional relationship between c and Δx such that the resulting covariance matrix is independent of the grid size as $\Delta x \to 0$ (or $q \to \infty$). This is the case for:

$$c = \exp\left[-\frac{1}{2}\left(\frac{\Delta x}{A}\right)^2\right] \approx 1 - \frac{1}{2}\left(\frac{\Delta x}{A}\right)^2, \tag{11}$$

where A is an arbitrary constant with a dimension of length and is defined as the correlation length of the random process. With that equation, we obtain from Eq. (1):

$$\frac{v_{i+1} + v_{i-1} - 2v_i}{(\Delta x)^2} - \frac{v_i}{A^2} = -\frac{a\left[2 + \left(\frac{\Delta x}{A}\right)\right]^2}{(\Delta x)^2}\xi_i = -\frac{2a}{c}\frac{\xi_i}{(\Delta x)^2}. \tag{12}$$

Denoting, in the limit of $\Delta x \to 0$, the first term as the second derivative of v with respect to $x, k = \frac{1}{A}$ and the forcing term by $f(x)$, we can recast Eq. (12) as the modified Helmholtz equation:

$$\frac{\mathrm{d}^2 v}{\mathrm{d}x^2} - k^2 v = f(x). \tag{13}$$

Since $f(x)$ is the limiting form of the set of random variables ξ_i defined on a discrete set of points, we take:

$$\sqrt{\Delta x}\xi_i = f(x_i)\Delta x, \tag{14}$$

i.e., $f(x)$ is a *white noise* process. This requires that a in Eq. (1) scales as $(\Delta x)^{3/2}$ in the limit where $\Delta x \to 0$.

Therefore, Eq. (1) becomes Eq. (13) as $\Delta x \to 0$ provided that we keep c as given by Eq. (11), and:

$$\begin{aligned} &a = a_1 \frac{c}{2}(\Delta x)^{3/2} \text{ with } a_1 \text{ to be an arbitrary constant,} \\ &\langle f(x_1) f(x_2)\rangle = a_1^2 \delta(x_1 - x_2). \end{aligned} \tag{15}$$

It is straightforward to solve Eq. (13) directly for the case where $v(x)$ is periodic with period L or for the case where $v(x)$ vanishes at the end point, i.e., $v(0) = v(L) = 0$. The solutions for $v(x)$ and the corresponding normalized covariance functions give:

(1) Periodic boundary conditions:

$$\begin{aligned} v(x) &= \frac{1}{2k\sinh\left(\frac{kL}{2}\right)}\int_0^L \mathrm{d}x_1 f(x_1)\cosh k(|x - x_1| - L/2), \\ \frac{\langle v(x)v(y)\rangle}{\langle v^2(x)\rangle} &= \{(Lk + k|y - x|(\cosh kL - 1) + \sinh kL)\cosh k(y - x) \\ &\quad + (1 - \cosh kL - k|y - x|\sinh kL]\sinh k|y - x|)\}/(Lk + \sinh kL). \end{aligned} \tag{16}$$

(2) For the case where $v(0) = v(L) = 0$:

$$\begin{aligned} v(x) &= \frac{1}{2k\sinh(kL)}\int_0^L \mathrm{d}x_1 f(x_1)[\cosh k(x + x_1 - L) - \cosh k(|x - x_2| - L)], \\ \langle v(x)v(y)\rangle &= \frac{1}{8k^3\sinh^2(kL)}[F(x - y) - F(x + y)], \end{aligned} \tag{17}$$

where $F(x) \equiv \sinh k|x| - \sinh k(|x| - 2L) + k|x|\cosh k(|x| - 2L) - k(|x| - 2L)\cosh kx$, here a_1 in (15) is set to 1.

Fig. 1 depicts the covariance function for the periodic case for different values of the ratio between the domain length L and the correlation length A. The cross points represent the numerical solution given by Eq. (11) and related equations. The number of grid points used for this plot is $m = 500$ (here not all the grid points are plotted) which gives a value of $c \approx 0.9988$ (cf. Eq. (11)) for the case with $L/A = 50$. The solid lines represent the analytical solutions (cf. Eq. (16)). There is a good agreement between the numerical and analytical results that suggests the scaling between c and Δx is correct. We have noticed that the absolute error between the analytical and numerical results for a given grid size, increase for

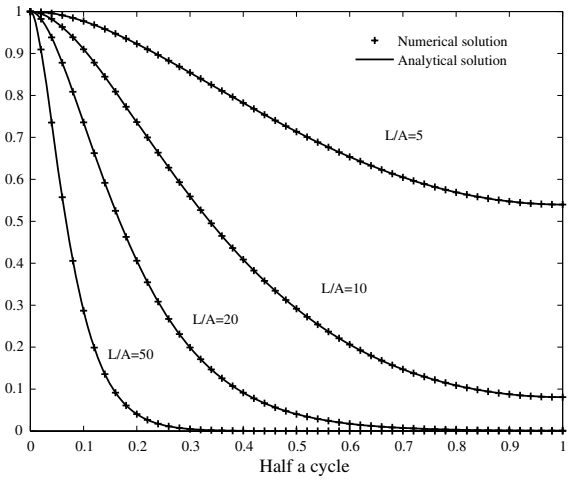

Fig. 1. 1D case – periodic: analytical and numerical representations of the covarianc kernel. L, domain length; A, correlation length.

increasing L/A. Moreover, the maximum errors occur in the correlation function region with maximum gradient, close to the origin. We have also verified (for a given L/A) that the finite difference scheme used to solve the Helmholtz equation was second-order: indeed the error decreases by a factor four when the equidistant grid is refined by a factor two (result not shown here).

Fig. 2 shows the variance for the second case where $v = 0$ at both end points for different values of L/A. Note in this case that the covariance is a function both of x and y. For brevity, we plot only its values along the diagonal of the covariance matrix. Therefore, this represents the variance of the process i.e., when $x = y$. The numerical method used here is a simple inversion of the coefficient matrix of v in Eq. (1). The scaling factor a_1 of Eq. (15) is taken to be $a_1 = 1$. Again, the good agreement between analytical and numerical results shows that both scaling factors in Eqs. (11) and (15) are relevant. The variance values in Fig. 2 are normalized by the maximum value of the covariance matrix. We list these values in Table 1.

(3) For the case where $v(0) = 0$ and $v(\infty)$ is finite:
$v(x)$ as governed by Eq. (13) can also be found as:

$$v(x) = \frac{1}{2k}\int_0^\infty \mathrm{d}x_1 f(x_1)\left[\mathrm{e}^{-k(x+x_1)} - \mathrm{e}^{-k|x-x_1|}\right]$$

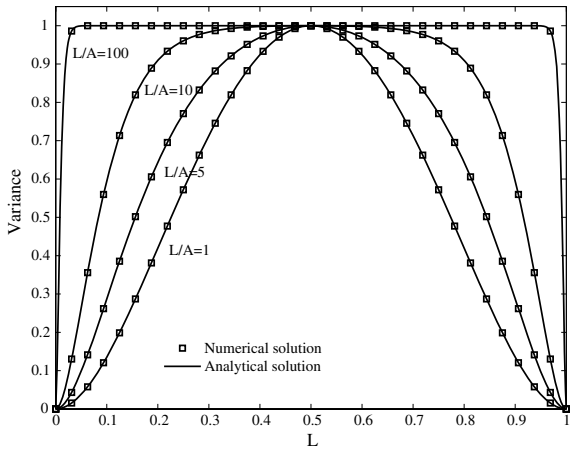

Fig. 2. 1D case – zero-Dirichlet: analytical and numerical representations of the variance. L, domain length; A, correlation length.

Table 1
Domain length $L = 1$, number of points $m = 1024$; $\max(k) =$ maximum element of the covariance matrix obtained by numerical computation

L/A	Δx	c	$\max(k)$	$\max(C)$	$\max\lvert k - C\rvert$
1	9.7656×10^{-4}	1.00000	0.0172	0.0172	3.0755×10^{-8}
10	9.7656×10^{-4}	0.99995	2.4974×10^{-4}	2.4975×10^{-4}	8.2465×10^{-9}
100	9.7656×10^{-4}	0.99524	2.4940×10^{-7}	8.2699×10^{-10}	8.2699×10^{-10}

$\max(C) =$ maximum element of the analytic covariance matrix obtained from Eq. (16).

and the corresponding covariance function is:

$$\langle v(x)v(y)\rangle = \frac{1}{4k^3}\left[(1+k|x-y|)\mathrm{e}^{-k|x-y|} - (1+k|x+y|)\mathrm{e}^{-k(x+y)}\right]. \tag{18}$$

3. Generalization to covariance functions in multi-dimensional domains

The correspondence between the discrete system of a random process governed by Eq. (1) and its continuous limit given by Eq. (13) can be easily extended to higher dimensions. The modified Helmholtz equation takes the following form:

$$\Delta v - k^2 v = f(\mathbf{x}), \tag{19}$$

where the Laplacian operator Δ represents the second-order derivative in multi-dimensions, and the random forcing term on the right-hand side is a *white noise* process function of the spatial position *vector* $\mathbf{x}$ and satisfying:

$$\langle f(\mathbf{x}_1)f(\mathbf{x}_2)\rangle = \delta(\mathbf{x}_1 - \mathbf{x}_2). \tag{20}$$

In two dimensions, the corresponding discrete system, written in its finite difference form, becomes:

$$\Delta v \Rightarrow \frac{v_{i+1,j} + v_{i-1,j} + v_{i,j+1} + v_{i,j-1} - 4v_{ij}}{(\Delta x)^2}, \tag{21}$$

here we assume $\Delta x = \Delta y$. Substituting this in Eq. (19), one obtains

$$v_{ij} = \frac{c}{4}(v_{i+1,j} + v_{i-1,j} + v_{i,j+1} + v_{i,j-1}) + a\xi_i\eta_j \quad \text{with } i,j = 1,2,\ldots,q \tag{22}$$

with

$$\begin{aligned} &c = \exp\left[-\frac{1}{4}(k\Delta x)^2\right], \\ &a\xi_i\eta_j = -\frac{c}{4}(\Delta x)^2 f(x_i,y_j) \text{ and } a = a_1\frac{c}{4}\Delta x, \end{aligned} \tag{23}$$

and ξ and η are iid random variables with zero mean and unit variance.

Similarly for three-dimensional problems, we will have the following discrete system:

$$v_{ijk} = \frac{c}{6}(v_{i+1,j,k} + v_{i-1,j,k} + v_{i,j+1,k} + v_{i,j-1,k} + v_{i,j,k+1} + v_{i,j,k-1}) + a\xi_i\eta_j\zeta_k \quad \text{with } i,j,k = 1,2,\ldots,q \tag{24}$$

with

$$\begin{aligned} &c = \exp\left[-\frac{1}{6}(k\Delta x)^2\right], \\ &a\xi_i\eta_j\zeta_k = -\frac{c}{6}(\Delta x)^2 f(x_i,y_j,z_k) \text{ and } a = a_1\frac{c}{6}(\Delta x)^{1/2}, \\ &\langle f(\mathbf{x}_1)f(\mathbf{x}_2)\rangle = \delta(\mathbf{x}_1 - \mathbf{x_2}) \end{aligned} \tag{25}$$

and where δ is a three-dimensional delta function.

3.1. Infinite domains

For infinite domains, the covariance function based on the modified Helmholtz equation can be readily obtained by taking the Fourier transform of Eq. (19). Letting

$$\begin{pmatrix} \hat{v}(\boldsymbol{\alpha}) \\ \hat{f}(\boldsymbol{\alpha}) \end{pmatrix} = \int \mathrm{d}^n x \mathrm{e}^{\mathrm{i}\boldsymbol{\alpha}\cdot\mathbf{x}} \begin{pmatrix} v(\mathbf{x}) \\ f(\mathbf{x}) \end{pmatrix}, \tag{26}$$

we obtain:

$$\hat{v}(\boldsymbol{\alpha}) = -\frac{\hat{f}(\boldsymbol{\alpha})}{\alpha^2 + k^2}. \tag{27}$$

We then invert it and obtain:

$$v(\mathbf{x}) = \int \mathrm{d}^n x_1 f(\mathbf{x}_1) G(\mathbf{x} - \mathbf{x}_1), \tag{28}$$

where the solution is represented as the convolution of the free space Green's function G with the forcing function f. We have:

$$G(\boldsymbol{\xi}, k^2) = -\frac{1}{(2\pi)^n} \int \mathrm{d}^n \alpha \frac{\mathrm{e}^{\mathrm{i}\boldsymbol{\alpha}\cdot\boldsymbol{\xi}}}{\alpha^2 + k^2}. \tag{29}$$

The covariance function is:

$$\langle v(\mathbf{x}) v(\mathbf{y}) \rangle = \int \mathrm{d}^n x_1 G(x - x_1) G(y - x_1) \tag{30}$$

(here we have used the orthogonality property of f).

In the present case, we have:

$$\begin{aligned} \langle v(\mathbf{x}) v(\mathbf{y}) \rangle &= \left(\frac{1}{2\pi}\right)^{2n} \int \mathrm{d}^n x_1 \int \mathrm{d}^n \alpha_1 \frac{\mathrm{e}^{\mathrm{i}\boldsymbol{\alpha}_1\cdot(x - x_1)}}{\alpha_1^2 + k^2} \int \mathrm{d}^n \alpha_2 \frac{\mathrm{e}^{\mathrm{i}\boldsymbol{\alpha}_2\cdot(y - x_1)}}{\alpha_2^2 + k^2} = \left(\frac{1}{2\pi}\right)^n \int \mathrm{d}^n \alpha \frac{\mathrm{e}^{\mathrm{i}\boldsymbol{\alpha}\cdot(\mathbf{x} - \mathbf{y})}}{(\alpha^2 + k^2)^2} \\ &= \frac{\partial}{\partial(k^2)} G(\mathbf{x} - \mathbf{y}; k^2) = \frac{1}{2k} \frac{\partial}{\partial k} G(\mathbf{x} - \mathbf{y}, k), \end{aligned} \tag{31}$$

where the Green's functions $G(\xi)$ for one, two and three dimensions are:

$$G_1(\xi) = \frac{-1}{2k} \mathrm{e}^{-k|\xi|}, \tag{32}$$

$$G_2(\boldsymbol{\xi}) = \frac{-1}{2\pi} K_0(k|\boldsymbol{\xi}|), \tag{33}$$

$$G_3(\boldsymbol{\xi}) = \frac{-1}{4\pi} \frac{1}{|\boldsymbol{\xi}|} \mathrm{e}^{-k|\boldsymbol{\xi}|}. \tag{34}$$

The covariance functions $C(\mathbf{x}, \mathbf{y}) = \langle v(\mathbf{x}) v(\mathbf{y}) \rangle$ becomes:

1. One-dimension:

$$C_1(x, y) = \frac{1}{4k^3} [1 + k|x - y|] \mathrm{e}^{-k|x-y|}. \tag{35}$$

2. Two-dimensions:

$$C_2(\mathbf{x}, \mathbf{y}) = -\frac{1}{4\pi k} K_0'(k|\mathbf{x} - \mathbf{y}|) \cdot |\mathbf{x} - \mathbf{y}| = \frac{|\mathbf{x} - \mathbf{y}|}{4\pi k} K_1(k|\mathbf{x} - \mathbf{y}|). \tag{36}$$

3. Three-dimensions:

$$C_3(\mathbf{x}, \mathbf{y}) = \frac{1}{8\pi k} \mathrm{e}^{-k|\mathbf{x}-\mathbf{y}|}, \tag{37}$$

where $K_0(x)$ and $K_1(x)$ are the modified Bessel functions of the zero and first order. We have used $K_1(x) = -K_0'(x)$. The two-dimensional results were obtained by Whittle [11]. Various finite domain applications can also benefit from this approach.

3.2. Finite domains

For finite domains, we need to solve the modified Helmholtz equation with some proper boundary conditions on the random process at the periphery of the domain. In the following, special attention is given to the two-dimensional case, as it is often the case that numerical simulations of three-dimensional physical systems in finite domains involve two-dimensional random inputs such as boundary conditions. For instance, in computational fluid mechanics, one could consider a two-dimensional random inflow boundary condition due to the turbulent fluctuations of the upstream flow. The uncertainty at the inlet could however vanish at the boundaries in case of internal flows such as duct or channel flows. From a physical point of view, it is therefore legitimate to have $v = 0$ at the boundary, if the random fluctuations are restricted to the interior of the domain but vanishes outside.

In one or higher dimensions, periodic boundary conditions are also reasonable ones, when the physical system is large but the (computational) domain of interest much smaller. We consider next both cases of periodic and zero Dirichlet boundary conditions.

In order to obtain the solution to Eq. (19), we first solve the following eigenvalue problem for the same computational domain, i.e.,

$$\begin{cases} \Delta\phi_n - \lambda_n^2\phi_n = 0 \quad \text{in } V, \\ \phi_n = 0 \quad \text{on } \partial V, \text{ or the periodic boundary conditions.} \end{cases} \tag{38}$$

It is easy to show that the eigenvalues λ_n^2 are non-negative and the eigenfunctions form a complete orthogonal set. We then use a normalized eigenfunction expansion to represent the functions $v(\mathbf{x})$ and $f(\mathbf{x})$ as follows:

$$\begin{aligned} v(\mathbf{x}) &= \sum_n a_n\phi_n(\mathbf{x}), \\ f(\mathbf{x}) &= \sum_n b_n\phi_n(\mathbf{x}) \text{ and } b_n = \int d^n x f(\mathbf{x})\phi_n(x), \end{aligned} \tag{39}$$

substituting in Eq. (19) we have:

$$a_n = -\frac{1}{\lambda_n^2 + k^2}\int \mathrm{d}^n x f(\mathbf{x})\phi_n(\mathbf{x}), \tag{40}$$

and

$$v(\mathbf{x}) = \int \mathrm{d}^n x_1 f(\mathbf{x}_1) G(\mathbf{x}, \mathbf{x}_1; k) \tag{41}$$

with

$$G(\mathbf{x}, \mathbf{x}_1, k) = -\sum_n \frac{\phi_n(\mathbf{x})\phi_n(\mathbf{x}_1)}{\lambda_n^2 + k^2}. \tag{42}$$

The corresponding covariance function is:

$$C(\mathbf{x}_1, \mathbf{x}_2) = \langle v(\mathbf{x}_1)v(\mathbf{x}_2)\rangle = \sum_n \frac{\phi_n(\mathbf{x}_1)\phi_n(\mathbf{x}_2)}{(\lambda_n^2 + k^2)^2} = \frac{1}{2k}\frac{\partial}{\partial k} G(\mathbf{x}_1, \mathbf{x}_2, k). \tag{43}$$

This has the same form as given in Eq. (31) for the case of infinite domain.

Let us use these formula and revisit the one-dimensional problem already solved by the direct method in the first section.

3.2.1. One dimensional case

(1) Periodic case:

Eigenvalues:

$$\lambda_0 = 0, \quad \lambda_n = \frac{2n\pi}{L} \quad \text{for } n = 1, 2, \ldots$$

Eigenfunctions:

$$\sqrt{\frac{1}{L}}, \quad \sqrt{\frac{2}{L}}\cos\frac{2n\pi}{L}x\sqrt{\frac{2}{L}}\sin\frac{2n\pi}{L}x \quad \text{for } n = 1, 2, \ldots$$

Green's function:

$$G(x_1, x_2; k) = -\frac{1}{L}\left[\frac{1}{k^2} + 2\sum_{n=1}^{\infty}\frac{\cos\frac{2n\pi}{L}(x_1 - x_2)}{\left(\frac{2n\pi}{L}\right)^2 + k^2}\right] = -\frac{1}{2k\sinh(kL/2)}\cosh k(|x_1 - x_2| - L/2). \tag{44}$$

Here, we have used the following formula:

$$\frac{1}{2} + \sum_{n=1}^{\infty}\frac{\cos\frac{2n\pi}{L}x}{1 + \left(\frac{2n\pi}{Lk}\right)^2} = \frac{Lk}{4\sinh(kL/2)}\cosh k\left(|x| - \frac{L}{2}\right).$$

The result checks with that given in Eq. (16).

(2) $v(0) = v(L) = 0$:

Eigenvalues:

$$\lambda_n = \frac{n\pi}{L} \quad \text{for } n = 1, 2, \ldots$$

Eigenfunctions:

$$\sqrt{\frac{2}{L}}\sin\frac{n\pi}{L}x, \quad \text{for } n = 1, 2, \ldots$$

Green's function:

$$G(x_1, x_2; k) = -\frac{2}{L}\frac{\sin\frac{n\pi}{L}x_1 \sin\frac{n\pi}{L}x_2}{\left(\frac{n\pi}{L}\right)^2 + k^2} = -\frac{1}{L}\sum_{n=1}^{\infty}\frac{\cos\frac{n\pi}{L}(x_1 - x_2) - \cos\frac{n\pi}{L}(x_1 + x_2)}{\left(\frac{n\pi}{L}\right)^2 + k^2}$$
$$= \frac{-1}{2k\sinh kL}[\cosh k(|x_1 - x_2| - L) - \cosh k(x_1 + x_2 - L)]. \tag{45}$$

Using the formula from Eq. (43), we obtain a covariance expression identical to the one given in Eq. (17).

3.2.2. Two-dimensional case

Let the 2D domain be a rectangle of size $L_1 \times L_2$.

(1) Periodic case:

Eigenvalues:

$$\lambda_{nm}^2 = \left(\frac{2m\pi}{L_1}\right)^2 + \left(\frac{2n\pi}{L_2}\right)^2 \quad \text{for } m, n = 0, 1, 2, \ldots \tag{46}$$

The eigenfunctions for each pair of m, n (not zeros) are fourfold degenerate:

$$\varphi_{mn} = \frac{2}{\sqrt{L_1 L_2}} \begin{cases} \cos\frac{2m\pi}{L_1} \times \cos\frac{2n\pi}{L_2} y, \\ \cos\frac{2m\pi}{L_1} \times \sin\frac{2n\pi}{L_2} y, \\ \sin\frac{2m\pi}{L_1} \times \cos\frac{2n\pi}{L_2} y, \\ \sin\frac{2m\pi}{L_1} \times \sin\frac{2n\pi}{L_2} y. \end{cases} \tag{47}$$

If either m or n (but not both) is zero, the eigenfunctions are doubly degenerate. They are:

$$\varphi_{m0} = \sqrt{\frac{2}{L_1 L_2}} \begin{cases} \cos\frac{2m\pi}{L_1} x, \\ \sin\frac{2m\pi}{L_1} x, \end{cases} \qquad \varphi_{0n} = \sqrt{\frac{2}{L_1 L_2}} \begin{cases} \cos\frac{2n\pi}{L_2} x, \\ \sin\frac{2n\pi}{L_2} x. \end{cases} \tag{48}$$

If both m, n are zero, there is a single eigenfunction:

$$\varphi_{00} = \frac{1}{\sqrt{L_1 L_2}}. \tag{49}$$

The covariance function becomes:

$$C(x_1, y_1, x_2, y_2) = \frac{4}{L_1 L_2} \sum_{m=1}^{\infty} \sum_{n=1}^{\infty} \frac{\cos\frac{2m\pi}{L_1}(x_1 - x_2) \cdot \cos\frac{2n\pi}{L_2}(y_1 - y_2)}{\left(\lambda_{mn}^2 + k^2\right)^2} + \frac{2}{L_1 L_2} \sum_{n=1}^{\infty} \left\{ \frac{\cos\frac{2n\pi}{L_1}(x_1 - x_2)}{\left[\left(\frac{2n\pi}{L_1}\right)^2 + k^2\right]^2} + \frac{\cos\frac{2n\pi}{L_2}(y_1 - y_2)}{\left[\left(\frac{2n\pi}{L_2}\right)^2 + k^2\right]^2} \right\} + \frac{1}{L_1 L_2} \frac{1}{k^4}. \tag{50}$$

(4) $v = 0$ on the boundary of a rectangle:
Eigenvalues and eigenfunctions:

$$\lambda_{nm}^2 = \left(\frac{m\pi}{L_1}\right)^2 + \left(\frac{n\pi}{L_2}\right)^2,$$

$$\varphi_{nm} = \frac{2}{\sqrt{L_1 L_2}} \left(\sin\frac{m\pi}{L_1} x\right) \left(\sin\frac{n\pi}{L_2} y\right)$$

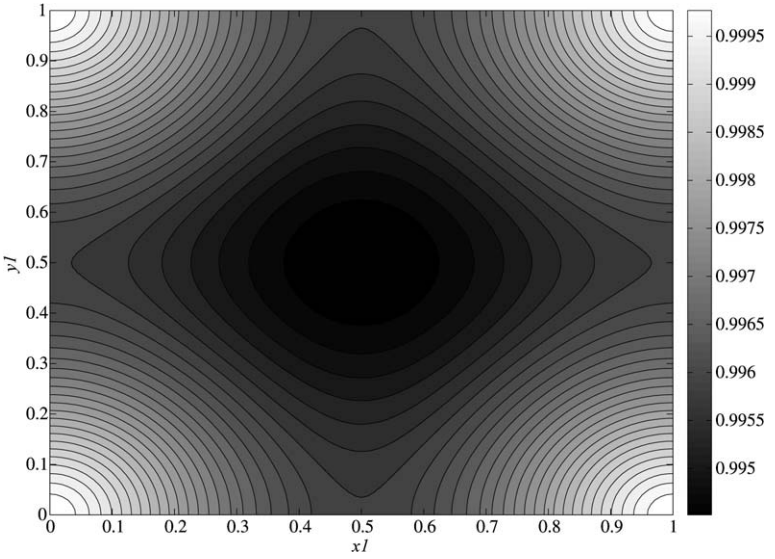

Fig. 3. 2D case – periodic: analytic representation of the covariance kernel $C(x_1, y_1, x_2 = 0, y_2 = 0)$; $L_1 = L_2 = 1$ and $k = 1/A = 1$.

and the corresponding covariance function is

$$C(x_1, y_1, x_2, y_2) = \frac{4}{L_1 L_2} \sum_{m=1}^{\infty} \sum_{n=1}^{\infty} \frac{\sin \frac{m\pi}{L_1} x_1 \sin \frac{m\pi}{L_1} x_2 \sin \frac{n\pi}{L_2} y_1 \sin \frac{n\pi}{L_2} y_2}{(\lambda_{nm}^2 + k^2)^2}. \tag{51}$$

All the above formula for the covariance functions involved convergent infinite or doubly infinite series. If $k = 1/A$ is large, i.e., when the correlation length is much smaller than the size of the domain, a large number of terms in the series will be needed to obtain accurate values of C.

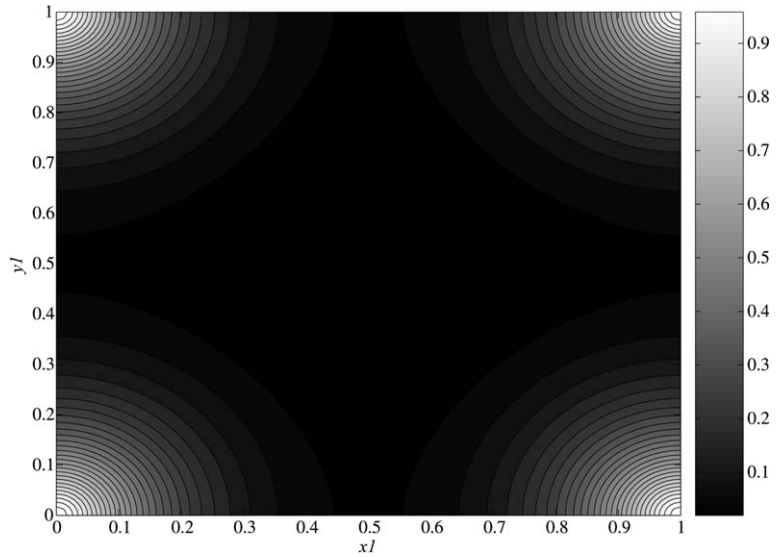

Fig. 4. 2D case – periodic: analytic representation of the covariance kernel $C(x_1, y_1, x_2 = 0, y_2 = 0)$; $L_1 = L_2 = 1$ and $k = 1/A = 10$.

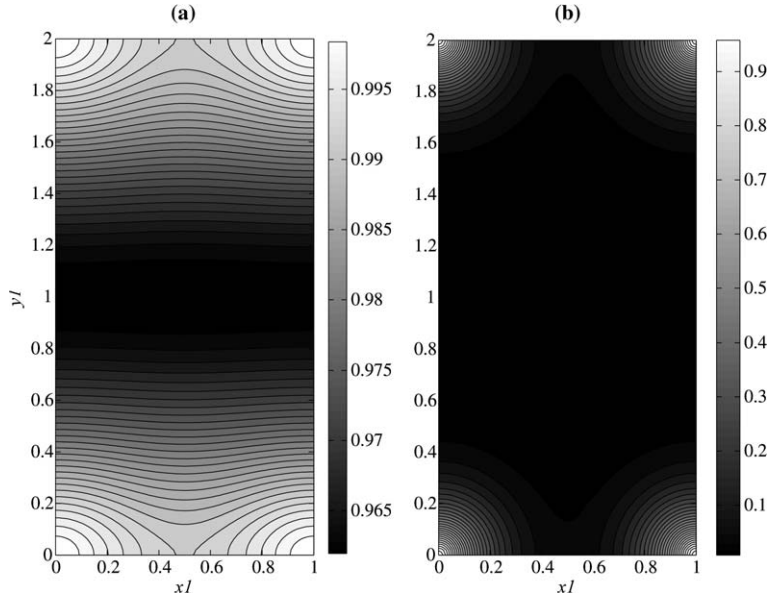

Fig. 5. 2D case – periodic: analytic representation of the covariance kernel $C(x_1, y_1, x_2 = 0, y_2 = 0)$; $L_1 = 1$ and $L_2 = 2$. (a) $k = 1/A = 1$; (b) $k = 1/A = 10$.

The finite sum approximation of this series is computed. In Fig. 3, we plot $C(x_1, y_1, x_2, y_2)$ of Eq. (50) by taking $x_2 = y_2 = 0$, $L_1 = L_2 = 1$, and $k = 1/A = 1$. The values of C are normalized by the maximum value of C, i.e. $C(0,0;0,0) \approx 1.0037$ in this case. We have used a 101×101 grid points and one hundred terms both for m and n.

Fig. 4 shows a somewhat different covariance kernel for $k = 10$ this time. In both cases the highest value happens at the four corners. The center region of the rectangle takes up the smallest value.

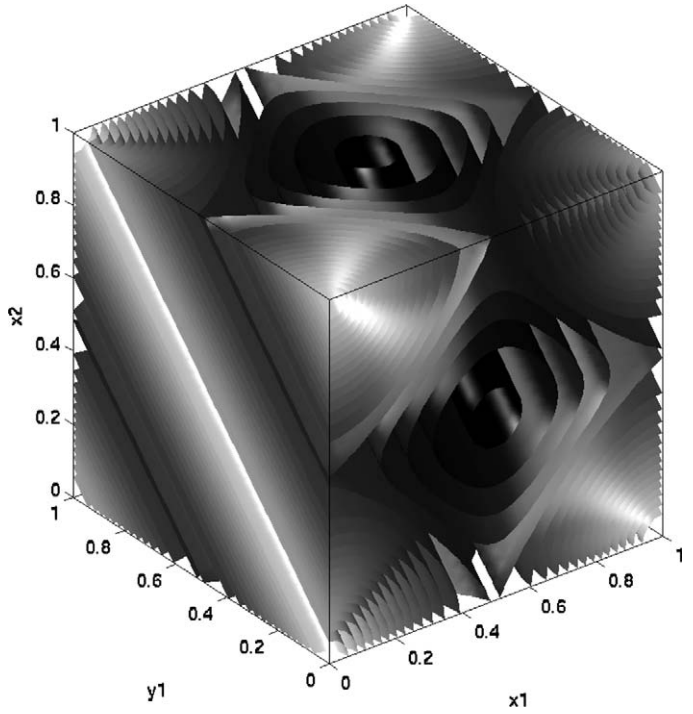

Fig. 6. 2D case – periodic: isosurfaces of the analytic representation of the covariance kernel $C(x_1, y_1, x_2, y_2 = 0)$; $L_1 = L_2 = 1$; $k = 1/A = 1$.

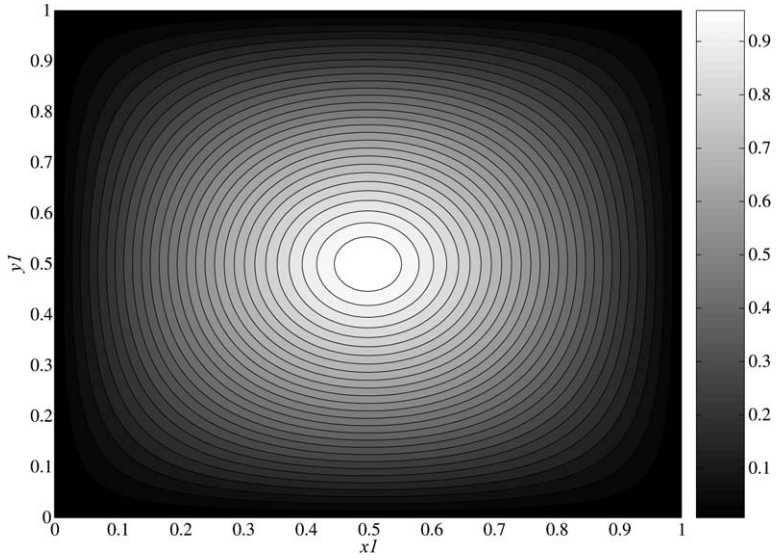

Fig. 7. 2D case – zero-Dirichlet: analytic representation of the covariance kernel $C(x_1, y_1, x_2 = L_1/2, y_2 = L_2/2)$; $L_1 = L_2 = 1$; $k = 1/A = 1$.

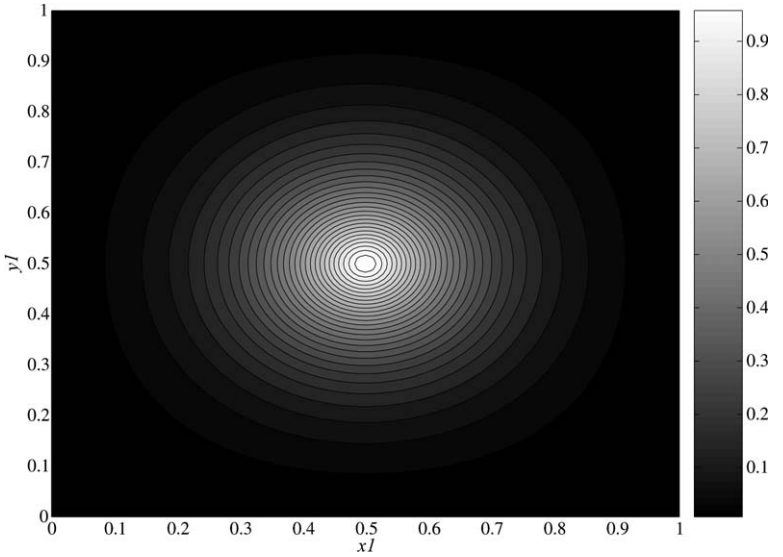

Fig. 8. 2D case – zero-Dirichlet: analytic representation of the covariance kernel $C(x_1, y_1, x_2 = L_1/2, y_2 = L_2/2)$; $L_1 = L_2 = 1$; $k = 1/A = 10$.

Fig. 5 show the corresponding covariance kernels for $L_1 = 1$ and $L_2 = 2$.

Fig. 6 shows isosurfaces of the covariance function $C(x1, y1, x2, y2 = 0)$ for $L_1 = L_2 = 1$ and $k = 1$. This figure relates to Fig. 3. We notice that the graph now becomes three-dimensional. It represents the covariance of an ensemble of points (line) with $(x_2 \in [0,1], y_2 = 0)$ with an ensemble of points (surface) with $((x_1, y_1) \in [0,1] \times [0,1])$. The dark surfaces represent the low covariance (darkest surface has a value of $C = 0.927$) and the light surfaces represent the large covariance (lightest surface has a value of $C = 0.995$). One can notice that the function is translational-invariant as expected.

Figs. 7 and 8 show the covariance kernel with the zero-Dirichlet boundary conditions for $k = 1$ and $k = 10$, respectively. The boundaries are not represented and only the values at the interior points of the domain are shown. Here, the values of C are normalized by the maximal value of C, i.e. $C(L_1/2, L_2/2; L_1/2, L_2/2) \approx 0.0106$ and $C(L_1/2, L_2/2; L_1/2, L_2/2) \approx 7.945 \times 10^{-4}$, respectively. In both cases the highest value is now obtained at the center of the rectangular domain and the covariance tends to zero at the boundaries. The center peak is sharper for larger k.

4. Numerical computation of the covariance kernels

In Section 2, we have carried out a direct numerical computation for the one-dimensional dynamical system (see Eq. (1)) and we have compared it with the analytical form (cf. the discussion of Figs. 1 and 2). Here, we reiterate a similar analysis for the two-dimensional version of the dynamical system (see Eq. (22)).

4.1. Formulation and validation

We first consider the periodic case which results in an easier representation of its covariance matrix because of the translational-invariant property. The resolution of the modified Helmholtz equation in two-dimensional domains has been treated in many papers. Traditional fast solvers, when based on the fast Fourier transform (FFT) [16,17], allow for uniform grids and simple geometry, while iterative methods (multigrid methods and domain decomposition techniques) handle unstructured grids and complex geometry [18,19]. Here, we do not necessarily need a very efficient solver but we need a method of discretization that preserves the property of orthogonality of the random forcing on the right-hand side of the equation (Eq. (20)). We make the choice to use a finite difference scheme that allows us to treat directly the values of the random process at the grid points. The modified Helmholtz equation with periodic boundary conditions (Eq. (19)) is discretized on a rectangular

2D cartesian grid with equidistant grid points using a second-order finite difference scheme (5-point stencil) and appropriate coefficients (Eqs. (22) and (23)). Following a classical finite difference representation, the random variables v_{ij} at the grid points are ordered and numbered in a single array sequence of size $n_1 \times n_2$, where n_1 and n_2 are the number of internal grid points along each direction respectively. Taking into account the periodicity at the boundaries, we construct the corresponding coefficient matrix of the v_{ij}. It takes the form of the following block matrix of size $n_2 \times n_2$ blocks:

$$B = \begin{pmatrix} a & b & 0 & 0 & \dots & 0 & b \\ b & a & b & 0 & \dots & 0 & 0 \\ 0 & b & a & b & \dots & 0 & 0 \\ 0 & 0 & 0 & 0 & \dots & a & b \\ b & 0 & 0 & 0 & \dots & b & a \end{pmatrix}, \tag{52}$$

where each block is a matrix of size $n_1 \times n_1$ elements. The diagonal block a is:

$$a = \begin{pmatrix} 1 & -\frac{c}{4} & 0 & 0 & \dots & 0 & -\frac{c}{4} \\ -\frac{c}{4} & 1 & -\frac{c}{4} & 0 & \dots & 0 & 0 \\ 0 & -\frac{c}{4} & 1 & -\frac{c}{4} & \dots & 0 & 0 \\ 0 & 0 & 0 & 0 & \dots & 1 & -\frac{c}{4} \\ -\frac{c}{4} & 0 & 0 & 0 & \dots & -\frac{c}{4} & 1 \end{pmatrix}, \tag{53}$$

and the block b is:

$$b = \begin{pmatrix} -\frac{c}{4} & 0 & 0 & \dots & 0 \\ 0 & -\frac{c}{4} & 0 & \dots & 0 \\ 0 & 0 & 0 & \dots & -\frac{c}{4} \end{pmatrix}. \tag{54}$$

Once the matrix of coefficients is inverted, we use the orthogonality property of the right-hand side (see Eq. (20)) to compute readily the covariance matrix of the solution. The computational advantage of this approach is that the *white noise* forcing does not need to be explicitly generated to compute the covariance. In order to maintain this efficiency, other numerical schemes (including numerical schemes based on unstructured grids) should be used as long as they preserve this property. Bearing in mind, the scaling relationships given in Eq. (23) for the two-dimensional case, we compare this numerical solution with the analytic solution obtained in the previous section. Fig. 9 shows the absolute error between the covariance obtained from the analytical approach and the numerical approach. The error is almost uniform over the domain with very small fluctuations. It was verified that the numerical solution approaches the analytic solution when the computational grid is refined.

4.2. Application to complex geometries

The numerical approach adopted above can be used for more complex geometries. As a first example, we consider now a L-shaped two-dimensional domain. The computational domain is the unit square with the $[0, L_1/2] \times [0, L_2/2]$ subdomain removed. Here, we solve the modified Helmholtz equation with zero Dirichlet boundary conditions at the boundaries of the L-shaped domain. We use the same numerical technique as described in the previous paragraph to discretize the domain and compute the covariance kernel. Fig. 10 shows the covariance kernel $C(x_1, y_1, x_2 = 3L1/4, y_2 = 3L_2/4)$ for $k = 1$ (a) and $k = 10$ (b) with $L_1 = L_2 = 1$ for both cases. The choice of the point $(x_2 = 3L_1/4, y_2 = 3L_2/4)$ is arbitrary. Here, there are 2581 grid points distributed on an equidistant L-shaped cartesian grid ($\Delta x = \Delta y = L_1/60$). For each case, the values of C are normalized by the maximum value of C over the domain, i.e. $C(3L_1/4, 3L_2/4; 3L_1/4, 3L_2/4) \approx 4.61 \times 10^{-3}$ for (a) and $C(3L_1/4, 3L_2/4; 3L_1/4, 3L_2/4) \approx 7.79 \times 10^{-4}$ for (b). As expected, the covariance values decay faster over the domain, away from the chosen point, for larger k.

Our second example is a hole-shaped two-dimensional domain. The physical domain is the unit square with the $\{(x_1 - L_1)^2 + (y_1 - L_2)^2 < R^2\}$ subdomain disk removed. The computational domain consists in the intersection between a uniform cartesian grid on the unit square and the disk geometry. Only the nodes of the grid

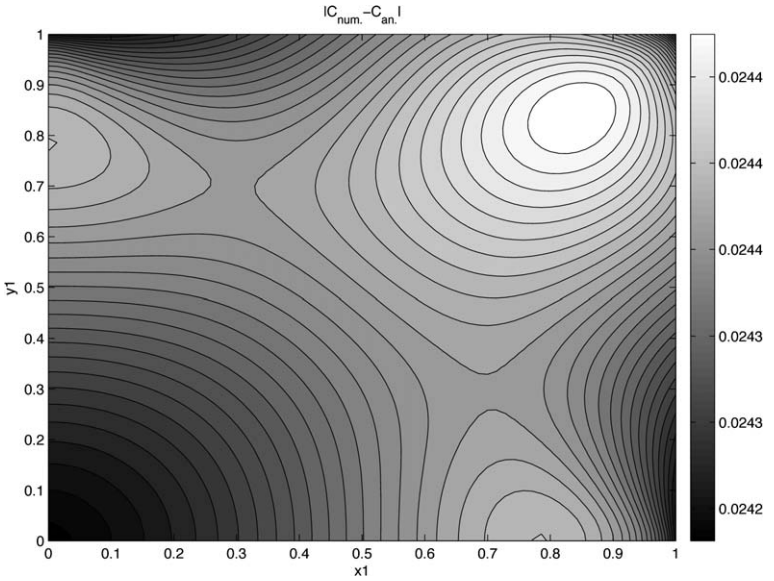

Fig. 9. 2D case – periodic: covariance kernel error between numerical and analytical solutions $C(x_1, y_1, x_2 = 0, y_2 = 0)$; $L_1 = L_2 = 1$; $k = 1/A = 1$.

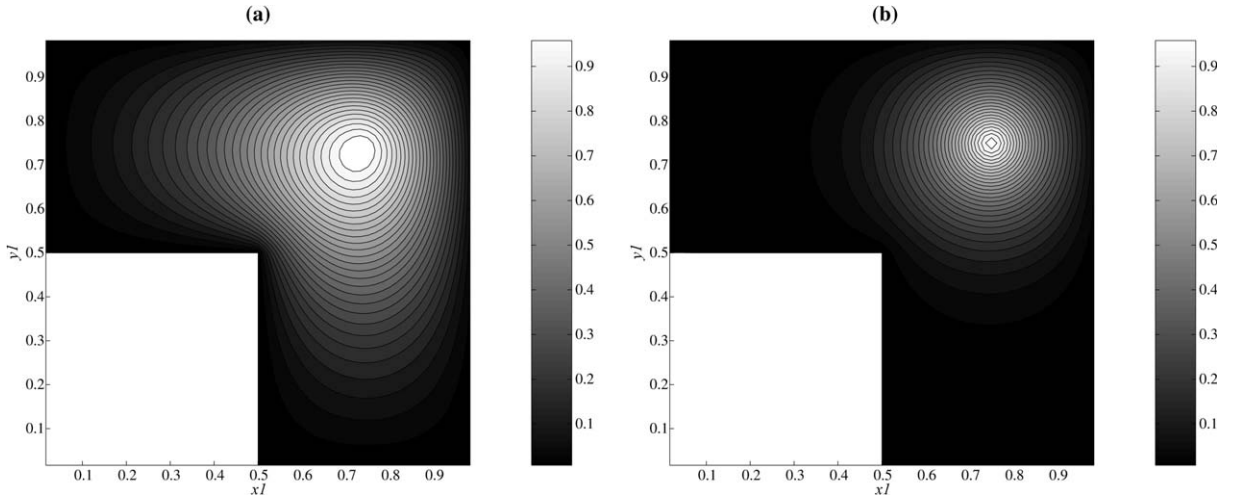

Fig. 10. L-shaped 2D case – zero-Dirichlet: numerical representation of the covariance kernel $C(x_1, y_1, x_2 = 3L1/4, y_2 = 3L_2/4)$; $L_1 = L_2 = 1$. (a) $k = 1/A = 1$; (b) $k = 1/A = 10$.

located outside of the disk are conserved. With this approach, the circular geometry is only approximated. The accuracy of the approximation is related to the number of grid points in each direction.

We solve again the modified Helmholtz equation with zero Dirichlet boundary conditions at the external and internal boundaries of the computational domain. We use the same numerical technique as described in the previous paragraph to construct the linear system and compute the covariance kernel. Here, the problem being a purely diffusive problem and the grid resolution being sufficiently fine, the effect of the grid irregularities on the solution is minor. We mention that a non-uniform grid (more adapted to the geometry) could be used in combination with a mapping function to transform it to a uniform grid. However, the accuracy of the solution on the non-uniform grid will depend strongly on the transformation. Fig. 11 shows the covariance kernel $C(x_1, y_1, x_2 = L1/4, y_2 = 3L_2/4)$ for $k = 1$ (a) and $k = 10$ (b) with $L_1 = L_2 = 1$ for both cases. The radius of the internal boundary is $R = L_1/10$. Here, there are 7488 grid points distributed on an equidistant cartesian

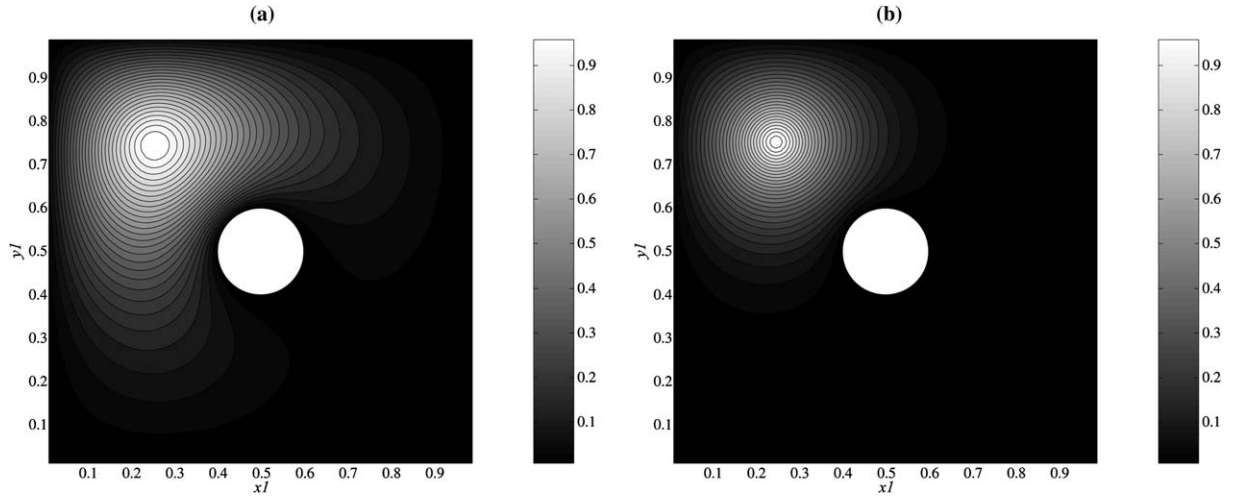

Fig. 11. Hole-shaped 2D case – zero-Dirichlet: numerical representation of the covariance kernel $C(x_1, y_1, x_2 = L1/4, y_2 = 3L_2/4)$; $L_1 = L_2 = 1$. (a) $L_1/A = 1$; (b) $L_1/A = 10$.

grid ($\Delta x = \Delta y = L_1/90$). For each case, the values of C are normalized by the maximum value of C over the domain, i.e. $C(L_1/4, 3L_2/4; L_1/4, 3L_2/4) \approx 3.68 \times 10^{-3}$ for (a) and $C(L_1/4, 3L_2/4; L_1/4, 3L_2/4) \approx 7.65 \times 10^{-4}$ for (b). As expected, the covariance values decay faster over the domain, away from the chosen point, for larger k.

5. Fourier series expansions and Karhunen–Loeve representation of a random process

In the eigenfunction expansion of the random process in Section 4, the sine and cosine functions come in predominantly. This is no surprise for the shape of the domain we considered there. One will expect that the eigenfunction expansion is really just the Fourier series expansion. Let us elucidate this point further by using the one-dimensional case. We represent a random process as a Fourier series:

$$v(x) = \frac{a_0}{\sqrt{2}}\xi_0 + \sum_{n=1}^{\infty}\left[\left(a_n \cos\frac{2n\pi}{T}x\right)\xi_n + \left(b_n \sin\frac{2n\pi}{T}x\right)\eta_n\right], \tag{55}$$

where ξ_n and η_n are iid random variables as seen before. Then we find for the covariance function:

$$\langle v(x_1)v(x_2)\rangle = \frac{a_0^2}{2} + \frac{1}{2}\sum_{n=1}^{\infty}\left[(a_n^2 + b_n^2)\cos\frac{2n\pi}{T}(x_1 - x_2) + (a_n^2 - b_n^2)\cos\frac{2n\pi}{T}(x_1 + x_2)\right]. \tag{56}$$

This defines the covariance functions as the *cosine* series. For the case that $v(0) = v(L) = 0$, we have $a_n = 0$. Taking the period $T = 2L$, we have:

$$\langle v(x_1)v(x_2)\rangle = \frac{1}{2}\sum_{n=1}^{\infty} b_n^2\left[\cos\frac{n\pi}{L}(x_1 - x_2) - \cos\frac{n\pi}{L}(x_1 + x_2)\right]. \tag{57}$$

Given the covariance function defined in Eq. (17), one can readily find the coefficient b_n^2 as:

$$b_n^2 = \frac{2}{Lk^4}\frac{1}{\left[1 + \left(\frac{n\pi}{Lk}\right)^2\right]^2} \tag{58}$$

which also checks with the expression given in Eq. (44).

Note that this is for the random process which satisfies the dynamical systems given in Eq. (1). The rate of convergence of the coefficients goes as n^{-4}. It is interesting to ask what kind of covariance function we will get if we require that the rate of convergence is exponentially fast, say $b_n^2 = a^n$ for $|a| < 1$. Now

$$\sum_{n=1}^{\infty} b_n^2 \cos n\theta = \sum_{n=1}^{\infty} a^n \cos n\theta = -\frac{1}{2}\left(1 - \frac{1 - a^2}{1 + a^2 - 2a\cos\theta}\right). \tag{59}$$

We find that:

$$\langle v(x_1)v(x_2)\rangle = \frac{a(1-a^2)\sin\frac{\pi}{L}x_1 \sin\frac{\pi}{L}x_2}{\left[1+a^2-2a\cos\frac{\pi}{L}(x_1-x_2)\right]\left[1+a^2-2a\cos\frac{\pi}{L}(x_1+x_2)\right]}, \tag{60}$$

so, as expected, it is an analytic function.

The representation of covariance functions as an infinite series in Eq. (56) or like those in Section 4 offers a direct representation of the random process $v(x)$ as a Karhunen–Loeve expansion as in the form of Eq. (55). Taking the covariance function in Eq. (56) as the kernel function for the eigenvalue problem over the interval L, i.e.,

$$\int_0^L \mathrm{d}x_1 \langle v(x)v(x_1)\rangle \psi(x_1) = \lambda\psi(x) \tag{61}$$

it is easy to see that the eigenvalues and eigenfunctions are:

$$\begin{aligned}
&\lambda_0 = \frac{a_0^2}{2}L, \quad \psi_0(x) = \frac{1}{\sqrt{L}},\\
&\lambda_{nc} = \frac{a_n^2}{2}L, \quad \psi_{nc}(x) = \sqrt{\frac{2}{L}}\cos\frac{2n\pi}{L}x,\\
&\lambda_{ns} = \frac{b_n^2}{2}L, \quad \psi_{ns}(x) = \sqrt{\frac{2}{L}}\sin\frac{2n\pi}{L}x.
\end{aligned} \tag{62}$$

With this eigenspectrum, Eq. (55) is simply the Karhunen–Loeve expansion. The same thing applies to all the covariance function obtained through the method of the eigenfunctions expansion done in Section 4.

6. Summary

We have demonstrated that the dynamical systems associated with the second-order stochastic processes governed by Eqs. (1), (22) and (24) in one-, two- and three-dimensional spaces lead to the modified Helmholtz equation (19) in the continuous limit of the grid size $\Delta x \to 0$. Moreover, the correlation constant c is related to the grid size and the correlation length A. The random forcings f in the discrete dynamical systems and the continuous analogue partial differential equations are given by Eqs. (14), (15), (23) and (25). We have used the modified Helmholtz equation to find the covariance functions for three different boundary conditions in one-dimensional domain. For infinite domains, we also obtained the explicit forms of the covariance functions in one, two and three dimensions. In Section 3.2, we used the eigenfunctions expansion to construct the covariance function in finite domains. The method is applicable to any geometry as long as one can obtain the corresponding eigenspectrum of the modified Helmholtz equation. We have worked out two cases explicitly for two-dimensional rectangular domains. In Section 4, we have used a direct numerical method to solve the two dimensional discrete dynamical systems with periodic boundary conditions or zero-Dirichlet boundary conditions. Simple as well as more complex geometrical domains have been studied. The results are compared with those obtained by the method of eigenfunctions expansion. This work should provide practical ways of incorporating spatially varying random processes into stochastic boundary-valued problems in science and engineering applications.

Acknowledgments

The first author acknowledges the support of ONR and NSF-ITR. We thank Pr. G. Karniadakis for his interest in the problem and his careful reading of the manuscript. Finally, but not least, our deep thanks to Mrs. Madeline Brewster for the preparation of the manuscript.

References

[1] W.L. Oberkampf, T.G. Trucano, C. Hirsch. Verification, validation, and predictive capability in computational engineering and physics, Technical Report SAND2003-3769, Sandia National Laboratories, 2003.

[2] Decision making under uncertainty, in: C. Greengard, A. Ruszczynski (Eds.), Series: The IMA Volumes in Mathematics and its Applications, vol. 128, Springer, Berlin, 2002.
[3] J. Glimm, D.H. Sharp, Prediction and the quantification of uncertainty, Physica D 133 (1999) 152–170.
[4] B. Bucciarelli, M.G. Lattanzi, L.G. Taff, Two-dimensional stochastic processes in astronomy, Astrophys. J. Suppl. Ser. 84 (1993) 91–99.
[5] C.W. Gardiner, Handbook of Stochastic Methods: For Physics, Chemistry and the Natural Sciences, second ed., Springer, Berlin, 1985.
[6] I. Karatzas, S.E. Shreve, Brownian Motion and Stochastic Calculus, Springer, Berlin, 1988.
[7] B. Oksendal, Stochastic Differential Equations. An Introduction with Applications, fifth ed., Springer, Berlin, 1998.
[8] T.T. Soong, M. Grigoriu, Random Vibration of Mechanical and Structural Systems, Prentice-Hall, Englewood Cliffs, NJ, 1993.
[9] D. Lucor, C.-H. Su, G.E. Karniadakis, Generalized polynomial chaos and random oscillators, Int. J. Numer. Meth. Eng. 60 (2004) 571–596.
[10] R.G. Ghanem, P. Spanos, Stochastic Finite Elements: A Spectral Approach, Springer, Berlin, 1991.
[11] P. Whittle, On stationary processes in the plane, Biometrika 41 (1954) 434–449.
[12] D. Lucor, Generalized polynomial chaos: applications to random oscillators and flow–structure interactions, Ph.D. Thesis, Brown University, 2004.
[13] C.-H. Su, D. Lucor, G.E. Karniadakis, Karhunen–Loève representation of periodic second-order autoregressive processes, in: G.D. van Albada, M. Bubak, P.M.A. Sloot (Eds.), Lecture Notes in Computer Science, vol. 3038, Springer, Heidelberg, 2004, pp. 827–834.
[14] M. Loève, Probability Theory, fourth ed., Springer, Berlin, 1977.
[15] D. Xiu, G.E. Karniadakis, Modeling uncertainty in steady state diffusion problems via generalized polynomial chaos, Comput. Meth. Appl. Math. Eng. 191 (2002) 4927–4948.
[16] B.L. Buzbee, G.H. Golub, C.W. Nielson, On direct methods for solving Poisson's equations, SIAM J. Numer. Anal. 7 (1970) 627–656.
[17] C. Canuto, M.Y. Hussaini, A. Quarteroni, T.A. Zang, Spectral Methods in Fluid Dynamics, Springer, Berlin/Heidelberg, 1988.
[18] S.F. McCormick, Multigrid Methods, Frontiers in Applied Mathematics, vol. 3, SIAM, Philadelphia, 1987.
[19] T.F. Chan, R. Glowinsky, J. Periaux, O.B. Widlund (Eds.), Domain Decomposition Methods, SIAM, Philadelphia, PA, 1989.